IET Microwaves, Antennas & Propagation

Research Article

IET Journals
The Institution of Engineering and Technology

Composite right–left-handed-based antenna with wide applications in very-high frequency–ultra-high frequency bands for radio transceivers

ISSN 1751-8725
Received on 20th December 2014
Revised on 5th July 2015
Accepted on 20th July 2015
doi: 10.1049/iet-map.2015.0308
www.ietdl.org

Mohammad Alibakhshi-Kenari[1] ✉, *Mohammad Naser-Moghadasi*[1], *Ramazan Ali Sadeghzadeh*[2]

[1]*Faculty of Engineering, Science and Research Branch, Islamic Azad University, Tehran, Iran*
[2]*Faculty of Electrical and Computer Engineering, K. N. Toosi University of Technology, Tehran, Iran*
✉ *E-mail: makenari@mtu.edu*

Abstract: This study presents a metamaterial-based antenna using the concept of composite right–left-handed transmission-lines. The radiation-cells layouts are based on L/F-shaped slits, so these slits are engraved on the radiation-patches for establishing a series-capacitor effect. Moreover, the radiation cells including the spirals and via-holes for the shunt-inductors implementation. By cascading the proper number of cells, the desired antennas for very/ultra-high frequency-bands are designed. The first-antenna with four L-shaped cells isconstructed on the Rogers_RO4003 substrate with thickness of 0.8 mm, so that each of cells occupies the size of 2.3 mm × 4.9 mm. This antenna covers the experimental-bandwidth of 0.2–1.8 GHz, which corresponds to 160% feasible-bandwidth. This antenna resonates at frequencies of 600–850–1200–1550 MHz, so highest gain and efficiency, happened at 1550 MHz, are 3.4 dBi and 88%. For improving the antenna performances, the second-antenna is modelled with one-cell more than first-antenna and with changing in the slit configuration to F-shape and increasing in the same substrate thickness to 1.6 mm. F-shaped antenna has size of 14.5 mm × 4.4 mm × 1.6 mm, covering a measured-bandwidth of 0.11–2.1 GHz with five resonance frequencies at 450–725–1150–1670–1900 MHz, which corresponds to 180.1% practical-bandwidth. Maximum of the measured gain and efficiency of antenna are 4.5 dBi and 95%, which occur at 1900 MHz.

1 Introduction

The antenna has become one of the most difficult challenges when designing the wireless communication systems in portable devices [1]. Owing to the limited space available for the antenna, shrinking conventional antennas may lead to performance degradation and complicated mechanical assembly. The meta-material (MTM) technology provides an opportunity to design an antenna with a smaller dimension at lower cost with better performance parameters at both the antenna and system levels [2, 3]. Various implementations of the MTM structures have been reported and demonstrated [4, 5]. In this paper, the MTM transmission lines (MTM-TLs) with periodic structures and N identical radiation unit cells cascading together have been investigated and applied, whereas each of cells are much smaller than one wavelength (λ) at the operational frequency. Composition of one MTM unit cell is categorised as a series inductor (L_R), series capacitor (C_L), shunt inductor (L_L) and shunt capacitor (C_R). L_L and C_L determine the left-handed (LH) mode propagation properties, whereas L_R and C_R determine the right-handed (RH) mode propagation properties. The composite RH/LH-TLs (CRLH-TLs) provide a conceptual route for implementing the small-size antennas. The CRLH-based antennas can also be made very wideband to support today's multiband wireless communication system needs. The electrical size of a conventional CRLH-TL is strongly related to its physical dimension and consequently reducing the device size usually once increasing the operational frequency. Physical size of an MTM is determined by four CRLH parameters; C_R, L_R, C_L and L_L. This property implies the following: if these four parameters are realised in a very compact form, the device size will be physically small [6, 7]. A typical realisation of CRLH-TL is found in a quasi-lumped TL with elementary cells consists of a series capacitor and a shunt inductor. As in practice, the normal shunt capacitance and series inductance cannot be avoided, so that C_R and L_R are RH parasitic effects created by spaces between strip and ground planes and unwanted currents flowing on the patches, respectively [8–10].

In this paper, the radiation resonating cells cascaded together based on MTM-TLs for antenna devices are designed, fabricated and tested. Design process of the cells is based on distributed implementation of the series capacitors and shunt inductors with new configurations of the slits and spirals. The radiation cells have benefits of miniaturised size, planar, low cost, low profile, ease of fabrication, light weight, capable for providing the broad bandwidth along with good radiation properties and ability for modelling the various slits with new configurations for the desired applications [11, 12]. The proposed L- and F-shaped antennas in this paper have same construction processes than the fabricated antennas in [11, 12], so just the slits shapes have been changed and well as the number of cells have varied relative to each other. On the basis of the parametric study presented in Section 3, these parameters, that is, number of unit cells and slits shapes in other words the slits dimensions have dramatic influences on proposed antennas performances such as dimensions, bandwidths, radiation specifications and resonance frequencies. In this paper, we want to design two antennas for radio applications with maximum size of 14×5 mm^2, which will be realised by changing the number of slits along with a variation in their layouts. Consequently, by tuning and optimising the structural parameters the antennas for desired applications with required dimensions to embedding on the portable telecommunication devices can be implemented. Therefore, as main feature of the proposed designs can be mentioned to their capability for working with a large number of slit shapes. Hence, regarding with Table 4 it can be inferred that differences and the originality of the proposed antennas in this paper compared with [11, 12] are their main characteristics such as compactness caused by variation in number of cells and too slits shapes, wider bandwidths (doubled in most cases), higher

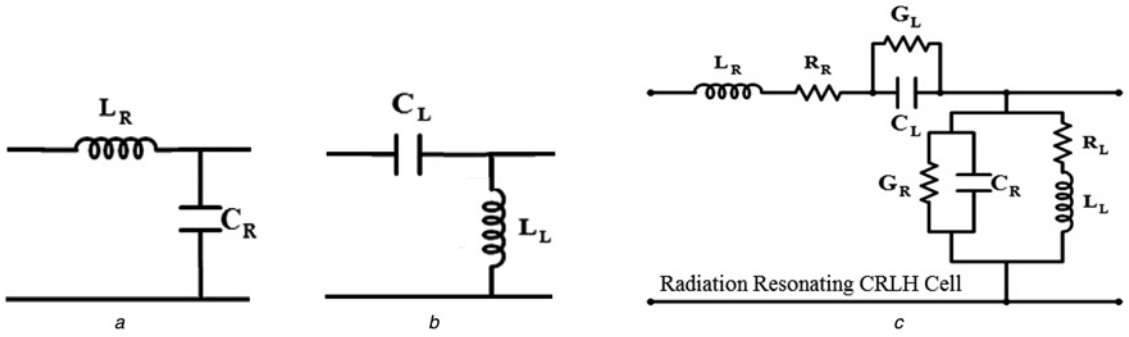

Fig. 1 *Circuit model of*

a Purely RH-TL
b PLH-TL
c Proposed radiation resonating cell based on the CRLH-TL with considering Losses

gains and efficiencies, better radiation patterns (patterns with omnidirectional properties in the *x*–*z*-plane and typical monopole patterns in the *x*–*y*-plane) and resonance frequencies, which more applicable them for wide applications compared with [11, 12]. Moreover, as another difference can be noted to the different substrates used in [11, 12] and this paper. The proposed MTM cells are copper and engraved directly on the dielectric substrate of Rogers_RO4003 with thicknesses of 0.8 and 1.6 mm.

This communication is arranged as follows. Section 2 presents the design processes of the radiation resonating cells for antenna devices, so this section is divided into three sections. Full circuit model of the structures along with their numerical analysis are discussed in Section 2.1 and the proposed L- and F-shaped antennas are designed in Sections 2.2 and 2.3, respectively. An analysis on antenna design parameters are elaborated in the next section. The antennas results are organised in Section 4. At last, conclusion is elaborated.

2 Design procedures

2.1 Full circuit model

The equivalent circuit model of the proposed radiation resonating cells based on CRLH-TL is shown in Fig. 1. It consists of C_L, L_L, C_R and L_R, which their dimensions are much less than the wavelength at operating frequency. Moreover, the structure losses are modelled by series resistance (R_R), shunt resistance (R_L), series conductance (G_L) and shunt conductance (G_R).

The circuit model of the purely LH-TL (PLH-TL) is shown in Fig. 1*b*, which is a dual of Fig. 1*a*. All series inductors in the RH-TL model are replaced by capacitors in the LH-TL model, and all shunt capacitors are substituted by inductors. It is an ideal model, which does not exist in nature. Circuit model of the proposed radiation resonating cell based on CRLH transmission, as is shown in Fig. 1*c*, is more suitable than the LH-TL circuit

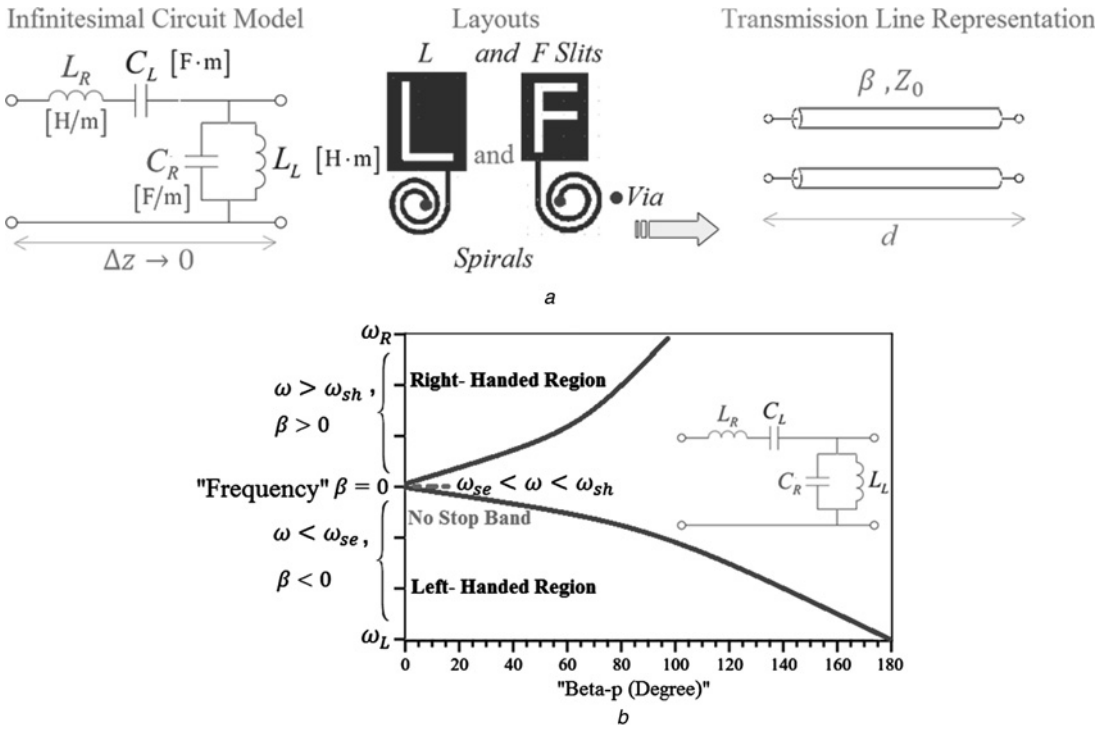

Fig. 2 *(a) Circuit model and layouts of the proposed radiation resonating CRLH-cells. C_L are implemented by the slits; L_L are implemented with the spirals; C_R are implemented by the gap spaces between trace and ground planes; L_R are implemented with the unwanted following of currents on the patches. (b) The dispersion diagram of the proposed radiation resonating CRLH-cells attained of the presented equations*

a Circuit model and layouts of CRLH unit cells
b Dispersion diagram of CRLH unit cells

IET Microw. Antennas Propag., 2015, Vol. 9, Iss. 15, pp. 1713–1726

model, since the parasite series inductance and shunt capacitance cannot be avoided in nature. It consists of series resonators of L_R and C_L and shunt resonators of C_R and L_L, where the subscript 'L' and 'R' denote LH and RH, respectively. The proposed circuit model is a combination of LH- and RH-TL. At low frequency, C_L and L_L are dominant, the TL shows the LH characteristics; at high frequency, L_R and C_R are dominant, the TL shows the RH characteristics (Fig. 2).

The proposed topologies based on CRLH-TLs are the periodic structures composed of the cascaded unit cells. These offered structures based on CRLH-MTM-TLs exhibit the propagation constant, γ symbol, as follows

$$\gamma = \alpha + j\beta = \sqrt{ZY} \tag{1}$$

with

$$\beta(\omega) = s(\omega)\sqrt{\omega^2 L_R C_R + \frac{1}{\omega^2 L_L C_L} - \left(\frac{L_R}{L_L} + \frac{C_R}{C_L}\right)} \tag{2}$$

where

$$s(\omega) = \begin{cases} -1, & \text{if} \quad \omega < \omega_{se} = \min\left(\dfrac{1}{\sqrt{L_R C_L}}, \dfrac{1}{\sqrt{L_L C_R}}\right) \\ 0, & \text{if} \quad \omega_{se} < \omega < \omega_{sh} \\ +1, & \text{if} \quad \omega > \omega_{sh} = \max\left(\dfrac{1}{\sqrt{L_R C_L}}, \dfrac{1}{\sqrt{L_L C_R}}\right) \end{cases} \tag{3}$$

and

$$Z(\omega) = j\left(\omega L_R - \frac{1}{\omega C_L}\right) \tag{4}$$

$$Y(\omega) = j\left(\omega C_R - \frac{1}{\omega L_L}\right) \tag{5}$$

where $\beta(\omega)$, $s(\omega)$, $Z(\omega)$ and $Y(\omega)$ are frequency functions and called as the dispersion relation, sign function, impedance and admittance of the antenna structures, respectively. Moreover, the series and shunt resonance frequencies are

$$\omega_{se} = \frac{1}{\sqrt{L_R C_L}} \tag{6}$$

$$\omega_{sh} = \frac{1}{\sqrt{L_L C_R}} \tag{7}$$

respectively.

Moreover, the phase and group velocities are defined as

$$v_p = \frac{\omega}{\beta} = \omega^2\sqrt{L_L C_L} \tag{8}$$

$$v_g = \left(\frac{\partial\beta}{\partial\omega}\right)^{-1} = \omega^2\sqrt{L_L C_L} \tag{9}$$

respectively. As well as, the dispersion diagram of the proposed radiation resonating CRLH cells is shown in Fig. 2*b*. The bandwidth of CRLH-TL unit cells is from high-pass LH cut-off frequency ω_L to low-pass RH cut-off frequency ω_R with no obvious stop-band and the broadband antennas are able to obtain. The cut-off frequencies ω_L and ω_R are given below

$$\omega_L = \frac{1}{\sqrt{L_L C_L}} \tag{10}$$

$$\omega_R = \frac{1}{\sqrt{L_R C_R}} \tag{11}$$

The cells are designed based on the engraved planar technology. In this way for implementing the radiation cells, the slits with new configurations and spirals are engraved on the planar patches by the standards manufacturing techniques. The designers have been modelled the slits with L- and F-shaped structures for implementing C_L. In addition, for establishing L_L the spirals have been employed, which are connected to ground plane through via holes. The benefits of cells are ease of implementation and low profile with capability designing the different configurations for use in various structures. In this design, by cascading the proper number of cells the desired antenna structures with wide applications in very-high frequency (VHF) and ultra-high frequency (UHF) bands for the radio transceivers are designed, constructed and measured.

The radiation unit cells are designed and built on Rogers_RO4003 substrate with dielectric constant of $\varepsilon_r = 3.38$, thicknesses of $h = 0.8$ and 1.6 mm and tan $\delta = 0.0022$. Each of L- and F-shaped unit cells occupies the area of $2.3 \times 4.9 \times 0.8$ mm^3 and $2.06 \times 4.4 \times 1.6$ mm^3, respectively. The cells are coupled together, so the structures from right side are fed by microstrip line and at other side are matched to 50 Ω load impedance of SMD1206 component connected to ground plane by via hole. The size of SMD1206 is 4.2 mm, so that its dimension has been considered in the total dimensions of antennas. The proposed MTM antennas consist of a feed line that is electromagnetically coupled to the metallic patches, slits, spirals and metallic via holes. This feed line through small slits stimulates the MTM radiation unit cells. To validate the design processes, the proposed structures are modelled by ANSOFT's three-dimensional (3D) full-wave electromagnetic field software called as high-frequency structure simulator (HFSS) [13] and after simulation and optimisation processes the antennas were fabricated and tested. Full discussion about the antennas design by the proposed radiation resonating CRLH cells are provided in the next sections.

2.2 MTM antenna with L-shaped slits

This antenna is combined of four simplified planar resonating cells based on CRLH-TLs and has been designed, tooled and fabricated on the Rogers_RO4003 substrate with thickness of 0.8 mm. Each of cells are composed of a host TL with one L-shaped slit engraved on the radiation patch by the standard manufacturing technique, and also a spiral inductor with two turns connected to ground plane through a metallic via hole. The L-shaped slits act like the C_L and the spiral inductors with metallic via holes act like the L_L. If we intentionally provide only C_L and L_L, the parasitic series RH inductance (L_R) and shunt RH capacitance (C_R) effects, increasing with increasing frequency, will unavoidably happen due to currents flowing in the metallisation and voltage gradients developing between the metal patterns of the strip and the ground planes, which indicates that these inductance and capacitance cannot be ignored. Thus, the CRLH model displays the most general MTM structure possible. In addition to these four reactive parameters, there are the conventional lossy parameters of R_R and G_R (RH) and the lossy parameters of G_L and R_L (LH), which account for the dielectric loss associated with C_L and the ohmic loss associated with L_L, respectively. Amounts of the antenna structural parameters including L_L, C_L, L_R, C_R, G_L, R_L, G_R and R_R were regulated and optimised by simulation processes in HFSS. The regulation and optimisation of the structural parameters are based on designing the suitable number of L-shaped slits, spiral inductors and via holes along with their proper dimensions. So that selecting the suitable number of cells with attention to size limitations for implementing the antenna with desired applications

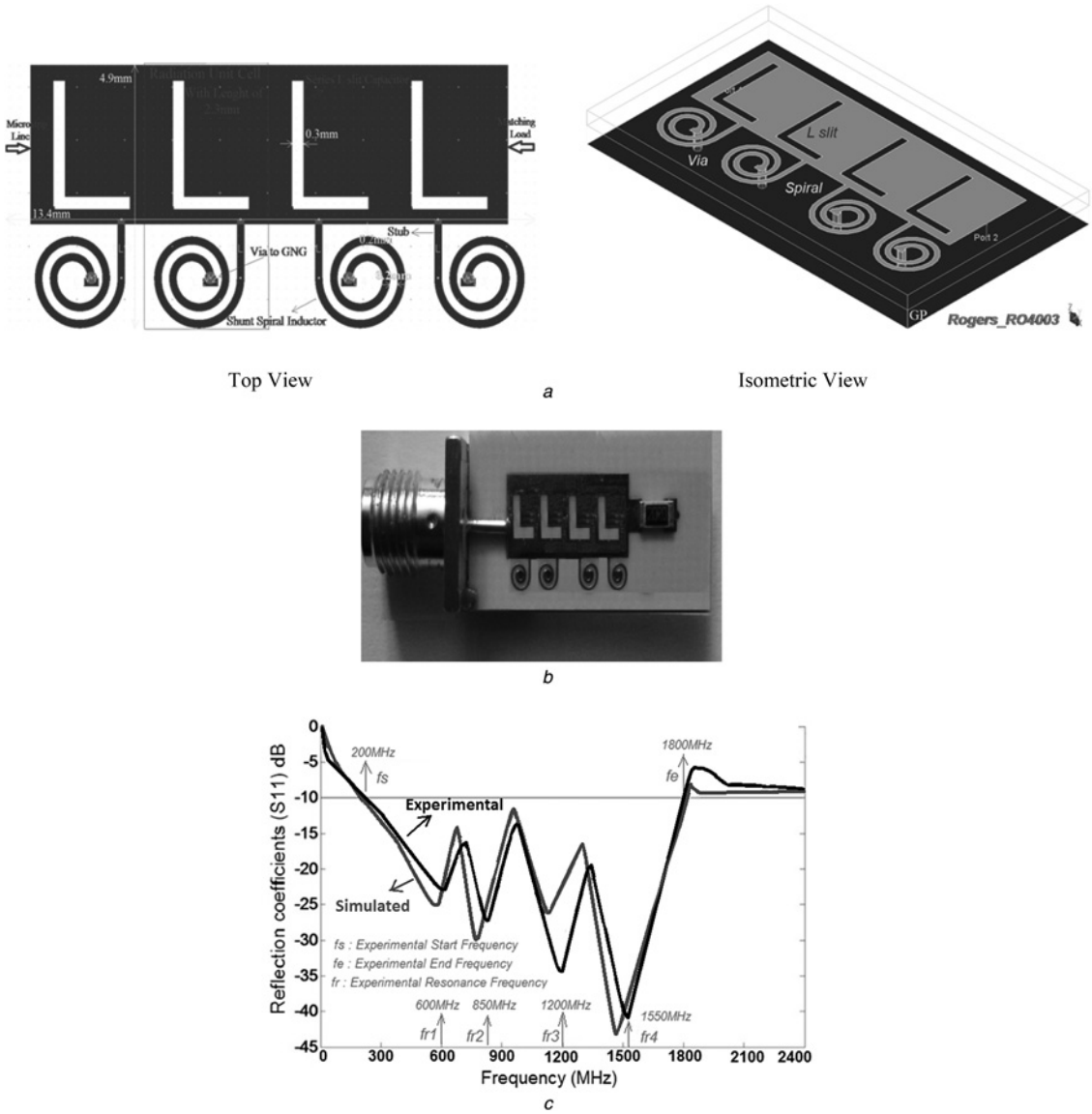

Fig. 3 *Formation of the L-shaped antenna with four cells made on the Rogers_RO4003 substrate with thickness of 0.8 mm (via height), (a) distributed implementation, (b) fabricated prototype and (c) reflection coefficients ($S_{11} < -10$ dB)*

a Distributed implementation
b Fabricated photograph
c Simulated (blue line) and experimental (black line) reflection coefficients ($S_{11} < -10$ dB)

has the dramatic influence on the antenna performances (explanations in details are elaborated in Section 3). In here, the designers want to model an antenna for application in VHF-band (30–300 MHz) and UHF-band (300 MHz–3 GHz). The antenna configuration is shown in Fig. 3.

For modelling and designing, the antenna is used of the MTM technology and the standard manufacturing techniques. With applying these techniques, the engraved slits on the radiation patches are realised, consequently a foot print area reduction is achieved. The total length, width and height of the L-shaped antenna are 13.4, 4.9 and 0.8 mm or $0.0089\lambda_0 \times 0.0032\lambda_0 \times 0.00053\lambda_0$, where λ_0 is free-space wavelength at 200 MHz. Since the antenna is composed of four cells with same dimensions, each of cells occupy the area of 2.3×4.9 mm^2.

Besides the small dimensions, the suitable bandwidth and good radiation properties are other main performance parameters in the antenna systems. To improve the bandwidth more cells are added. In this paper, the designers for extending the size have been provided a tradeoff between size with bandwidth and radiation properties. So that with employing the suitable number of inductive and capacitive elements, an acceptable small size with capability of presenting the desired bandwidth and good radiation properties is obtained. We have been selecting four radiation cells for implementing the L-shaped antenna in this stage.

The L-shaped antenna exhibited in Fig. 3 provides 1625 MHz bandwidth of 195 MHz–1.82 GHz obtained of HFSS and 1600 MHz bandwidth of 200 MHz–1.8 GHz reached of measurement, for voltage standing wave ratio (VSWR)≤2, which corresponds to 160% practical bandwidth. The reflection coefficients ($S_{11} < -10$ dB) of the antenna are indicated in Fig. 3. As is clear of Fig. 3, the antenna resonates at four operational frequencies including 600, 850, 1200 and 1550 MHz. The experimental gains and efficiencies of the antenna at aforementioned frequencies are 1.2 dBi and 34% at 600 MHz, 1.7 dBi and 45% at 850 MHz, 2.1 dBi and 62% at 1200 MHz and 3.4 dBi and 88% at 1550 MHz. Experimental 2D and 3D radiation patterns of the antenna at various resonance frequencies are plotted in Figs. 4*a* and *b*. Moreover, the experimental curves of the antenna gain and efficiency versus frequency are exhibited in Fig. 4*c*.

The simulated and measured radiation patterns of the antenna at operating frequencies in the two principle planes, the *x*–*z* and *x*–*y* planes are shown in Fig. 4. The antenna has approximately

IET Microw. Antennas Propag., 2015, Vol. 9, Iss. 15, pp. 1713–1726

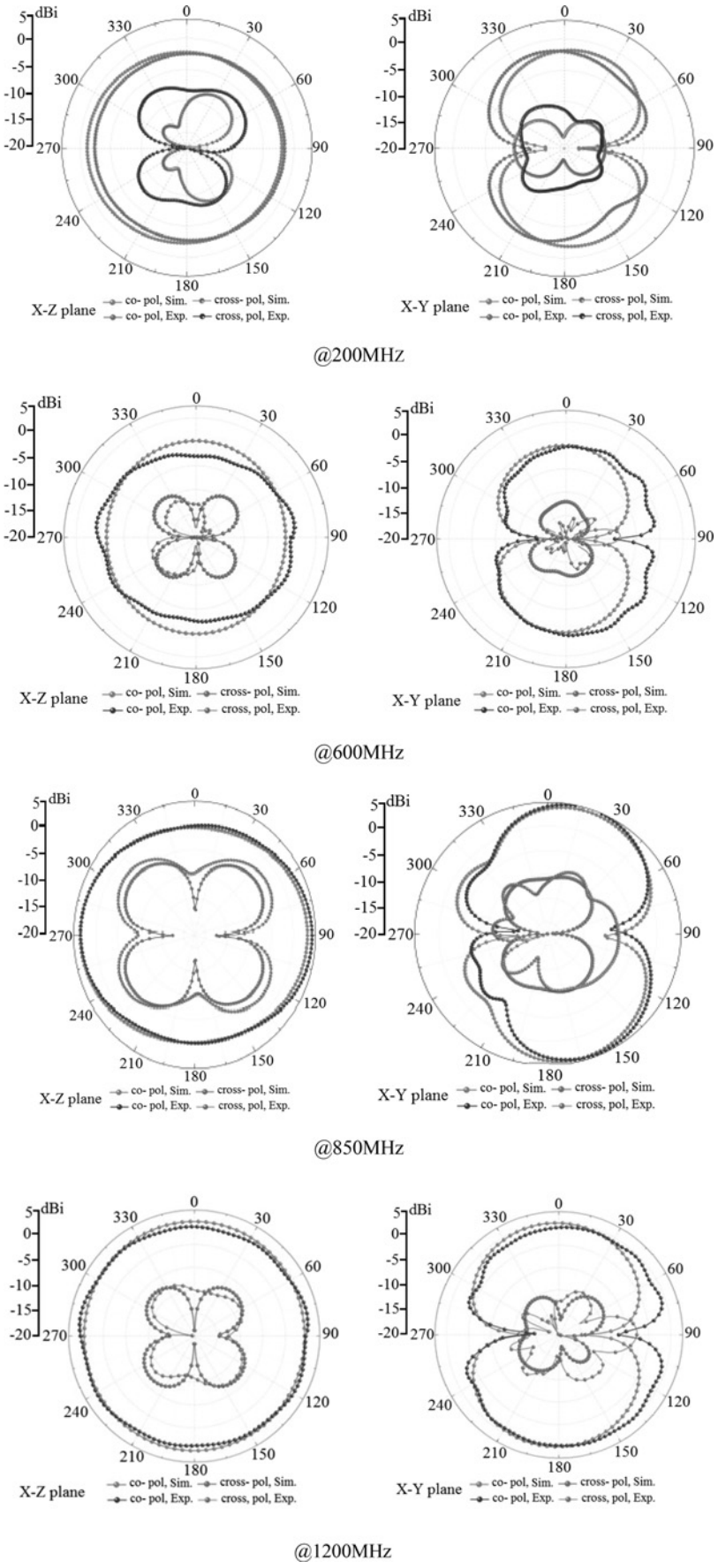

Fig. 4 *Experimental radiation patterns and curves of the L-shaped antenna (a) 2D patterns, dynamic range is dBi, (b) 3D patterns and (c) antenna gain and efficiency curves*

a 2D radiation patterns
b 3D radiation patterns
c Gain and efficiency curves versus frequency

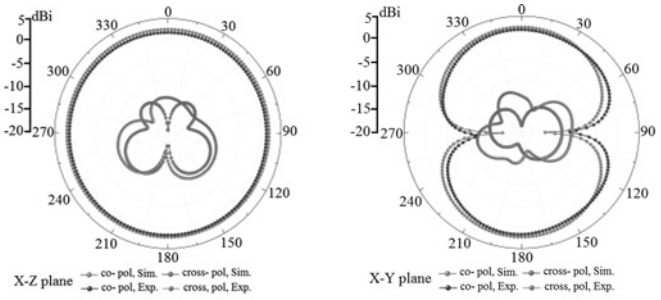

@1550MHz

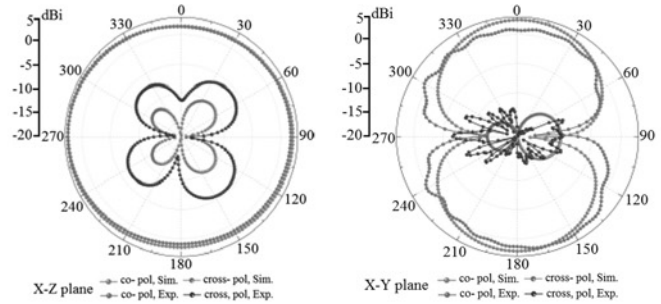

@1800MHz

a

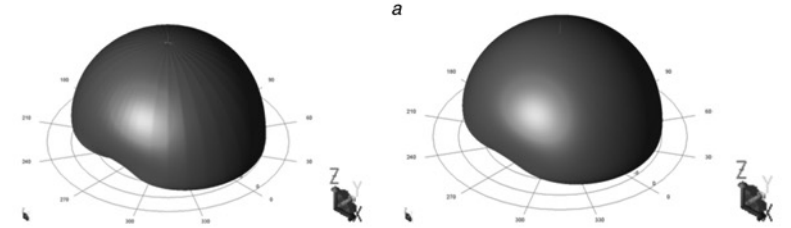

f_{r1}:600MHz f_{r2}:850MHz

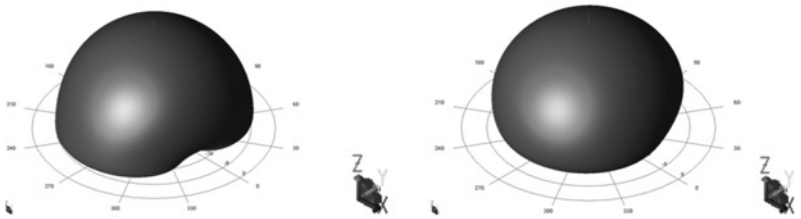

f_{r3}:1.2GHz f_{r4}:1.55GHz

b

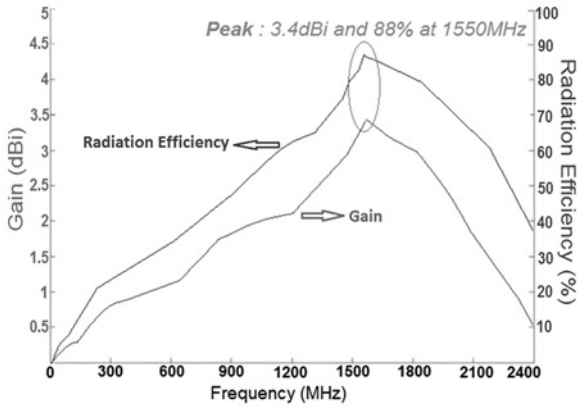

c

Fig. 4 *Continued*

IET Microw. Antennas Propag., 2015, Vol. 9, Iss. 15, pp. 1713–1726

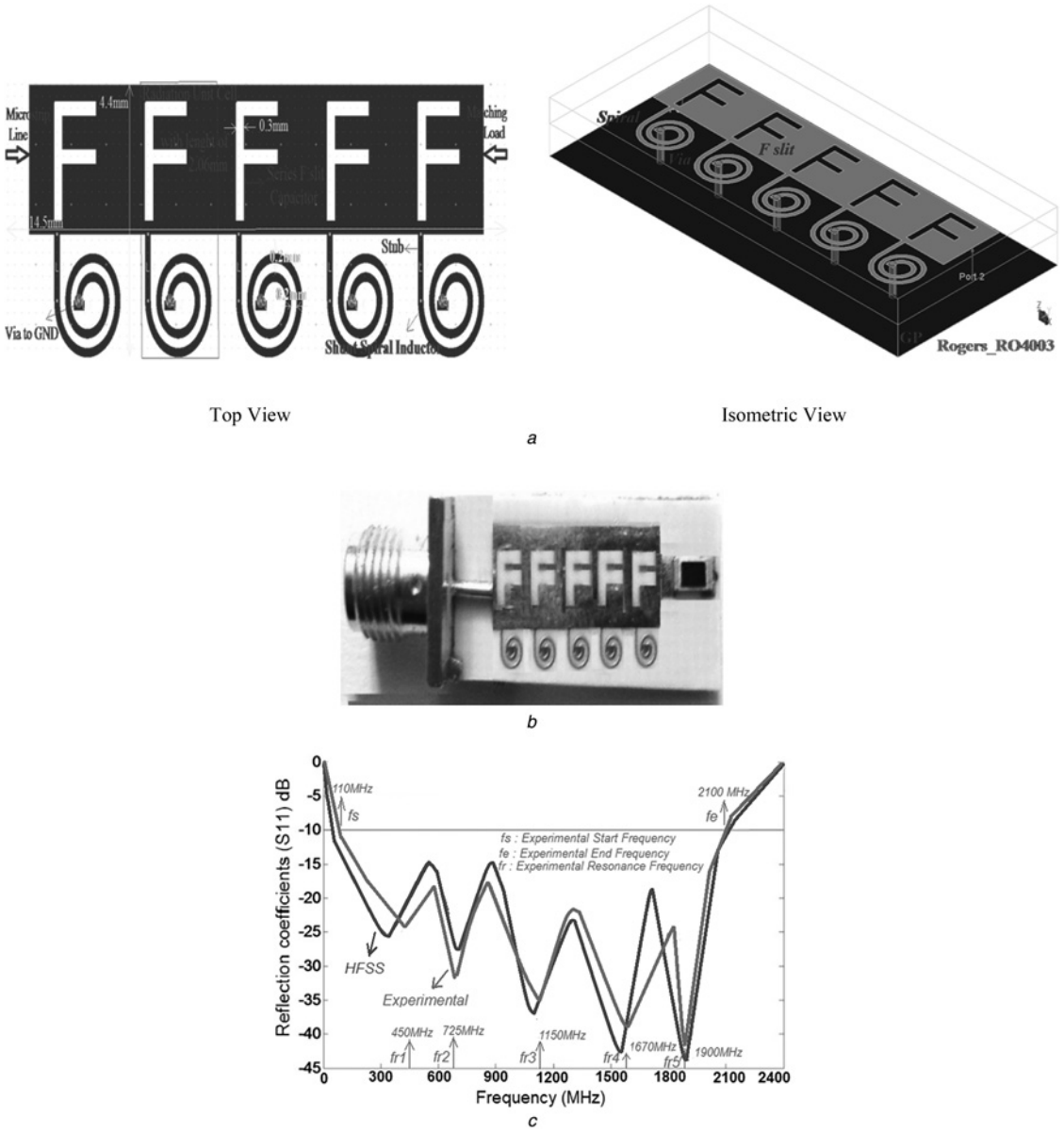

Fig. 5 *Configuration of the antenna with five F-shaped cells constructed on the Rogers_RO4003 with thickness 1.6 mm (via height). (a) Distributed implementation, (b) fabricated photograph and (c) reflection coefficients ($S_{11} < -10$ dB)*

a Distributed implementation
b Fabricated prototype
c Simulated (blue line) and experimental (red line) reflection coefficients ($S_{11} < -10$ dB)

omnidirectional radiation patterns in the x–z-plane. The x–y-plane patterns show two nulls at the y-direction, which are similar to that of a typical monopole antenna.

2.3 MTM antenna with F-shaped slits

In this section, the design goal is modelling and implementing an antenna with better specifications than the L-shaped antenna. Hence, the antenna layout is modified by changing the slits configurations to F-shaped structures and also one more radiation cell is employed compared with the L-shaped antenna. Consequently, the F-shaped antenna is constructed by cascading five radiation cells. Similar to previous section, the structural parameters of F-shaped antenna is regulated and optimised by HFSS and after simulations the antenna was fabricated and tested. The antenna circuit model is shown in Figs. 1 and 2.

The antenna configuration is exhibited in Fig. 5. Clearly, the antenna is constructed of five radiation cells. As a result, the antenna size is increased than to first-antenna with four cells, accordingly, by increasing the cells the bandwidth and radiation specifications of F-shaped antenna increase in comparison with L-shaped antenna. The total dimension of the antenna is $14.5 \times 4.4 \times 1.6$ mm^3 or $0.0053\lambda_0 \times 0.0016\lambda_0 \times 0.00058\lambda_0$, where λ_0 is free-space wavelength at 110 MHz. Since the antenna is combined of five cells, each of them occupies the area of $0.00075\lambda_0 \times 0.0016\lambda_0$ at 110 MHz (2.06×4.4 mm^2).

It is notable that, besides increasing the number of cells to five and changing the cells layout for improving the bandwidth and radiation characteristics, the designers have been enhancing the thickness of substrate (height of via hole) to 1.6 mm (double the first case), which has a positive influence on the bandwidth and radiation specifications. Hence, the F-shaped antenna is designed and fabricated on the Rogers_RO4003 substrate with thickness of 1.6 mm. The antenna covers the impedance bandwidths of 90 MHz–2.14 GHz from HFSS and 110 MHz–2.10 GHz from measurement for VSWR$\leq$2, which corresponding to 180.1% operating bandwidth. The reflection coefficients ($S_{11} < -10$ dB) of

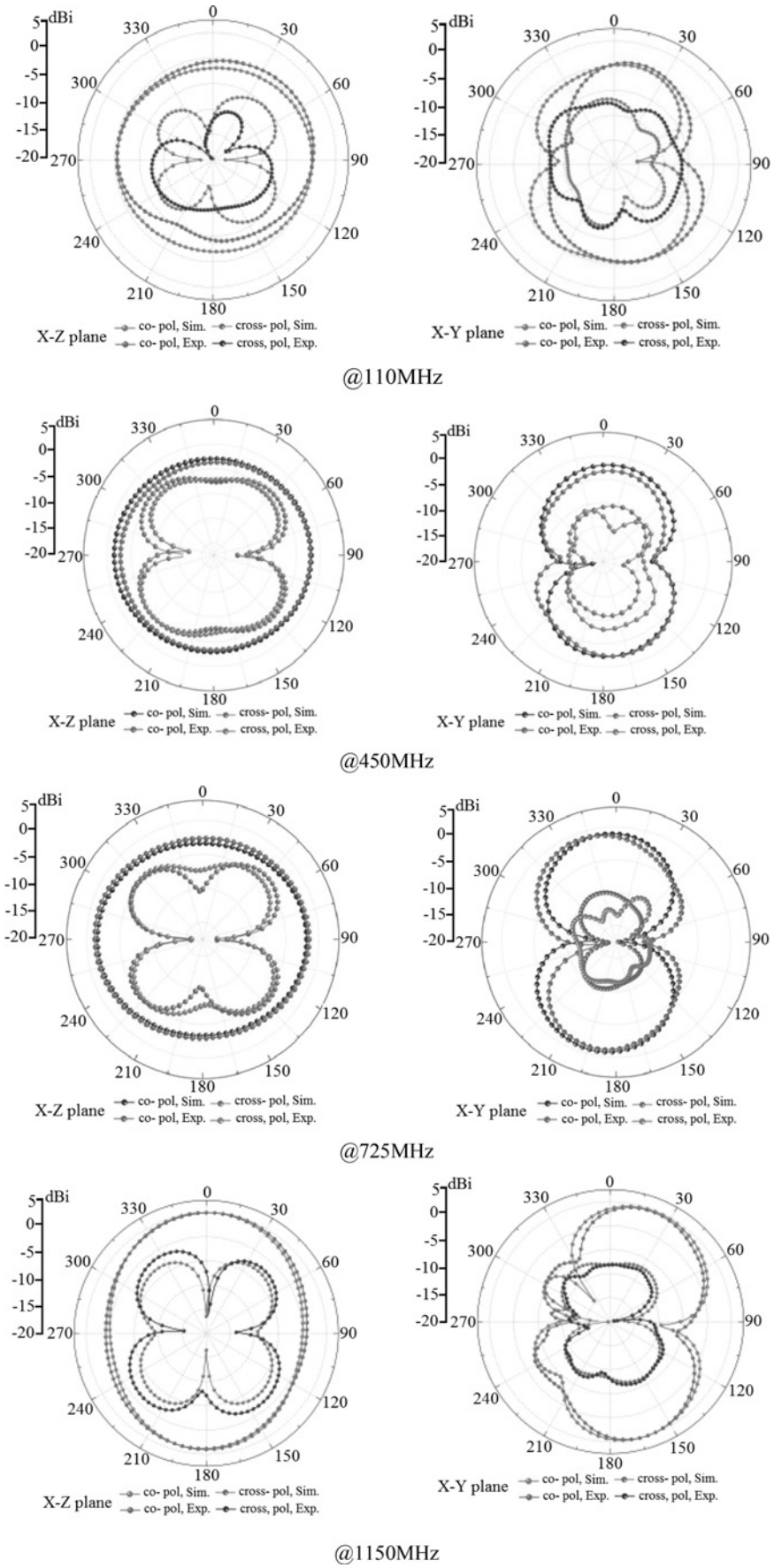

Fig. 6 *Experimental radiation patterns and curves. (a) 2D patterns, dynamic range is dBi, (b) 3D patterns and (c) gain and efficiency curves*

a 2D radiation patterns
b 3D radiation patterns
c Gain and efficiency curves versus frequency

IET Microw. Antennas Propag., 2015, Vol. 9, Iss. 15, pp. 1713–1726

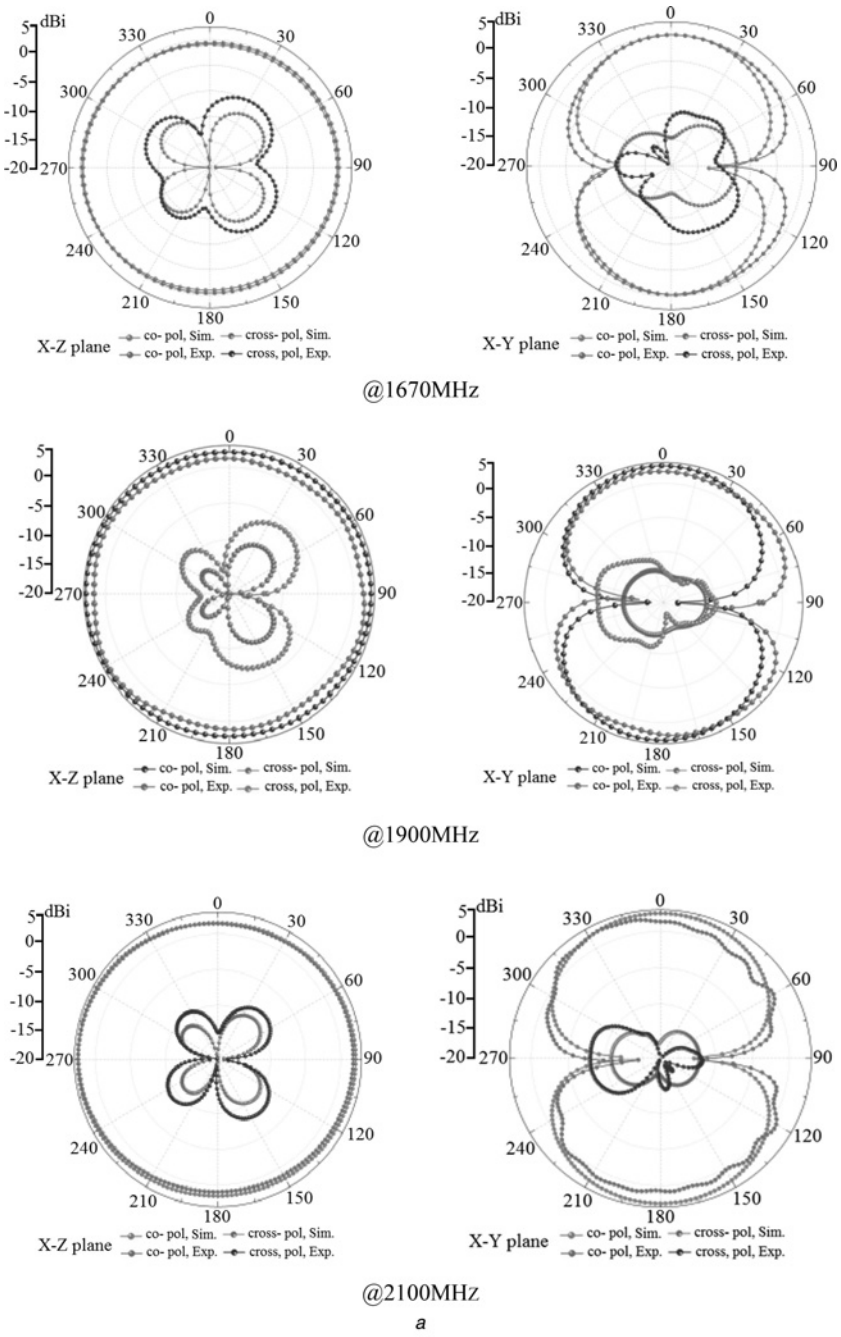

a

Fig. 6 *Continued*

the antenna are displayed in Fig. 5. The antenna resonates at five frequencies of 450, 725, 1150, 1670 and 1900 MHz. The experimental gains and efficiencies of the F-shaped antenna at above frequencies are 1.0 dBi and 31% at 450 MHz, 1.8 dBi and 47% at 725 MHz, 2.5 dBi and 70% at 1150 MHz, 3.8 dBi and 89% at 1670 MHz and 4.5 dBi and 95% at 1900 MHz. Experimental 2D and 3D radiation patterns at operating resonance frequencies are plotted in Figs. 6*a* and *b*. As well as, the experimental curves of antenna gain and efficiency versus frequency are exhibited in Fig. 6*c*.

The simulated and measured radiation patterns of the antenna at the operational frequencies and in the vertical and horizontal cuts, that is, in the *x*–*z* and *x*–*y* planes are shown in Fig. 6. It can be seen that the measured radiation patterns agree well with the simulated results. For wide band applications, an omnidirectional radiation pattern is normally preferred (i.e. in the *x*–*z*-plane). The results of Fig. 6 show that the radiation patterns in the entire band satisfy this requirement well. In the *x*–*y*-plane, the radiation patterns in Fig. 6 show two nulls occurring at the positive and negative *y* directions, which is typical for monopole antennas.

3 Analysis on antenna design parameters

To validate the results of both proposed antennas, the simulated specifications of design parameters which are number of unit cells, dimensions of L-and F-shaped slits along with spirals dimensions and numbers of spiral turns are expressed. Unit cells, slits and spirals characteristics are studied by ANSYS HFSS simulation tool.

3.1 L-antenna

To provide the desired performances, the number of unit cells, dimensions of the L-shaped slits accompanying the dimensions

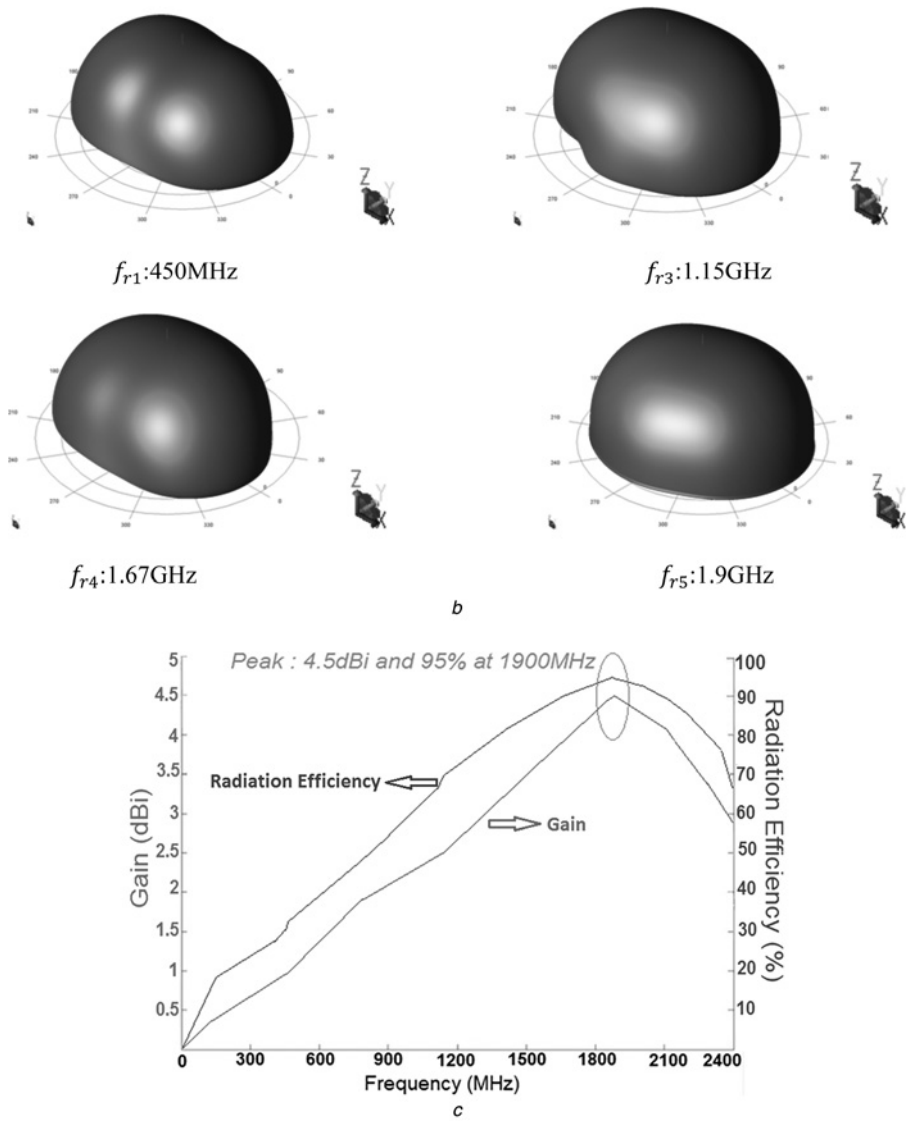

Fig. 6 *Continued*

and number of turns of spirals have optimised and regulated using ANSYS HFSS EM simulator. Figs. 7*a–c* explain the effects of these parameters on the reflection coefficients ($S_{11} < -10$ dB) of the proposed L-shaped antenna for various number of cells (n), lengths of slits (L_S) and widths of slits (W_S).

The criteria used to determine the number of CRLH-TL unit cells depend on a tradeoff between the antenna dimensions, impedance bandwidth and radiation characteristics. The overall goal here was to design and implement an antenna that had a maximum length of 14 mm and exhibited a wide bandwidth with good omnidirectional radiation patterns. The number of unit cells was determined through optimisation using HFSS. Fig. 7*a* shows the reflection coefficient of the antenna with increasing number of unit cells from 1 to 4. Four unit cells provide the widest impedance bandwidth of 1625 MHz for a reflection coefficient of −10 dB. It can be seen that the number of cells has a major influence on number of resonance frequencies, so that by increasing the number of cells the resonance frequencies of designed antenna has enhanced. Therefore, four unit cells were used here in the antenna design. The results of the parametric study, that is, slit length and width, are shown in Figs. 7*b* and *c*, respectively. The results show a greater slit length enhances the impedance bandwidth of the antenna. In fact an enhancement of the slit length from 1.5 to 2.5 mm increases the bandwidth of 1150–1625 MHz for reflection coefficient of −10 dB. The slit width has the effect on the impedance matching, that is, an enhancement of slit width from 0.2 to 0.3 mm results in an improve of the impedance matching to better than −42 dB. The optimised number of cells, length and width of the L-shaped slit were determined from these results to be 4, 2.5 mm and 0.3 mm, respectively.

Besides the requirement of compact size and wide bandwidth, the antenna needed to possess good radiation characteristics such as gain and efficiency. It is well known that the extension of the effective aperture of the antenna improves its gain and efficiency performance. Conventionally, this can be achieved by increasing the effective cross-sectional area of antenna. The proposed antenna's effective aperture was increased by simply increasing the number of CRLH-TL unit cells, which is confirmed in Figs. 7*d* and *e*. Antenna with one unit cell provides a peak gain and efficiency of 0.4 dBi and 12%, respectively, at 1450 MHz. Increasing the unit cells from one to four results in peak gain and efficiency improvement to 3.4 dBi and 88%, respectively, at 1550 MHz.

After analysis the structural parameters, that is, the number of cells, lengths and widths of slits, other main parameters are spirals. Hence, a parametric study on spiral characteristics is elaborated. Please note that in our designs the main influences of spirals are on antennas radiation characteristics, Fig. 7*f*. As clear, with increasing the W_{SP}, S_{SP} and N_{SP} the antenna gain and efficiency have been improved. This is realised due to increasing the effective cross-sectional area of antenna by extending the spiral dimensions.

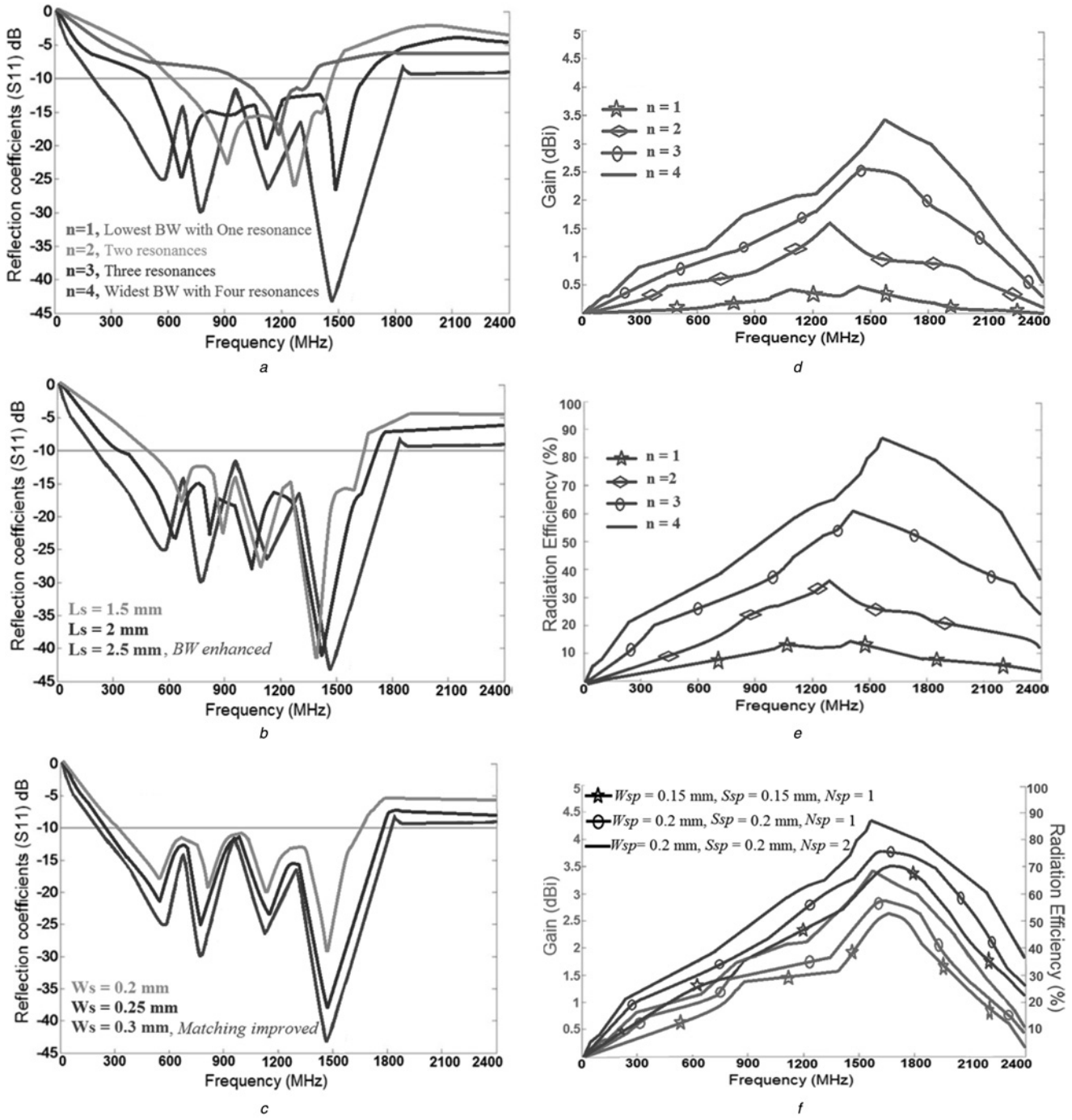

Fig. 7 *(a–c) Reflection coefficient (S_{11}) response of the proposed antenna as a function number of the design parameters, (d and e) gain and efficiency performance as a function of number of CRLH-TL unit cells and (f) gain and efficiency response as a function of W_{SP}, S_{SP} and N_{SP}*

a Reflection coefficient (S_{11}) response of the proposed antenna as a function of number of cells. Bandwidth is improved from BW = 31.75% for one cell up to BW = 160% when using 4-cells, as well as the resonance frequencies are increased by enhancing the number of cells

b Reflection coefficient (S_{11}) response of the antenna as a function of the slit length. The slit width was kept fixed at 0.3 mm

c Reflection coefficient (S_{11}) response of the antenna as a function of the slit width. The slit length was fixed at 2.5 mm

d Antenna gain versus frequency with variation in number of unit cells ($n = 1$–3 are in simulations and $n = 4$ is in measurements)

e Antenna efficiency versus frequency with variation in number of unit cells ($n = 1$–3 are in simulations and $n = 4$ is in measurements)

f Gain and efficiency response as a function of spiral widths (W_{SP}), distances between spiral rings (S_{SP}) and number of spiral turns (N_{SP}) ($N_{SP} = 1$ and $N_{SP} = 2$ are for simulated and measured cases, respectively)

3.2 F-antenna

Same analysis is done on the design parameters of F-shaped antenna (Fig. 8). It can be seen that the desired performances are achieved by an optimisation similar with L-shaped antenna.

As can be seen from results, the regulation and optimisation of the structural parameters are based on designing the suitable number of slits and spirals along with their proper dimensions. So that selecting the suitable number of cells with attention to size limitations for implementing the antenna with desired applications has the dramatic influence on the antenna performances.

Fig. 8 illustrates better results in comparison with the previous version; its main reason is increase in number of unit cells, increase in thickness of same substrate, that is, height of via hole and changing slits layouts from L to F shapes. Consequently, it can be found from results that the proposed antenna can work with a large number of slit shapes for required applications.

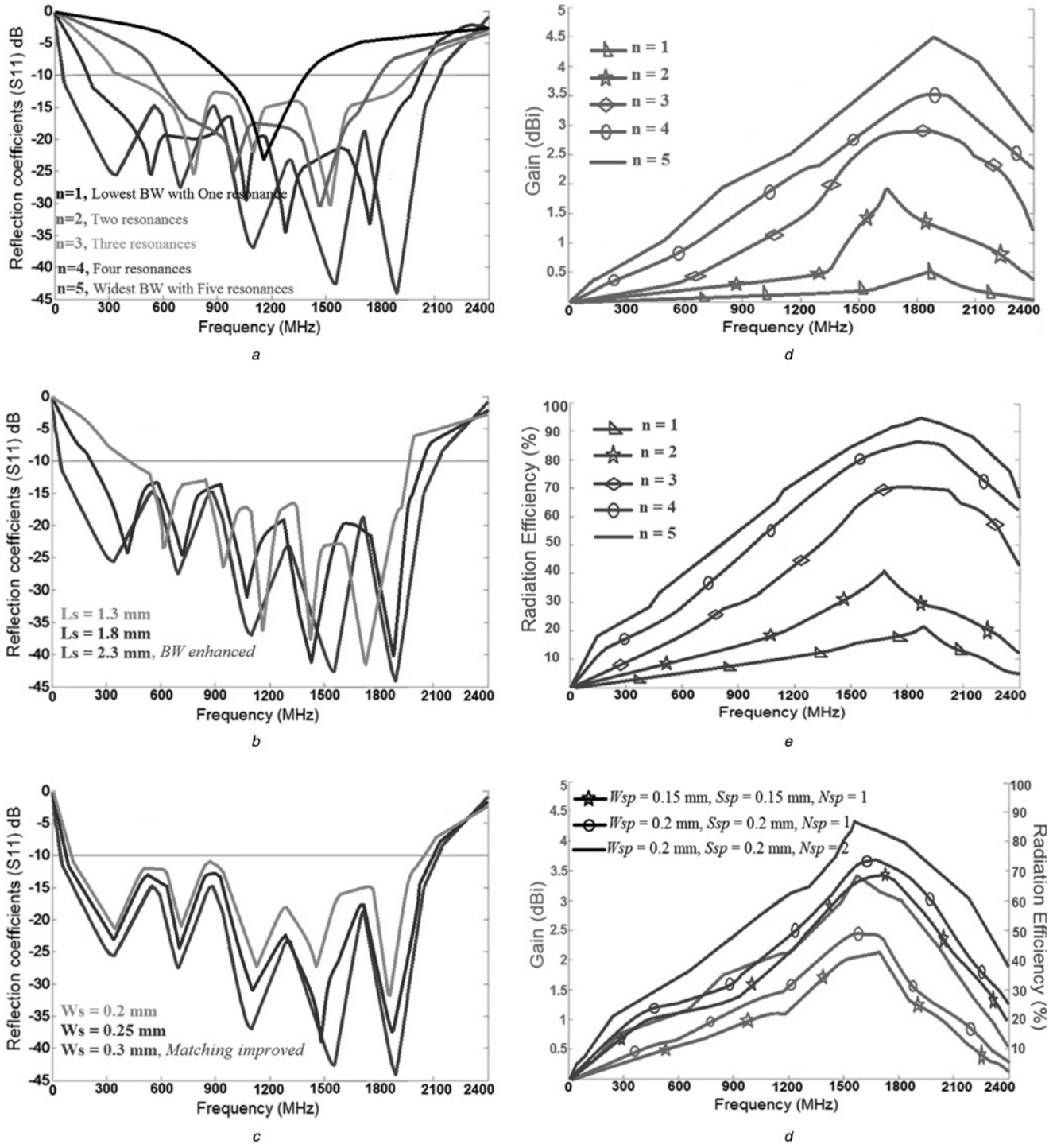

Fig. 8 *Parametric study on design parameters of F-shaped antenna*

a Reflection coefficient (S_{11}) response of the proposed antenna as a function of number of cells. Bandwidth is improved from BW = 43.47% for one cell up to BW = 180.10% when using 5-cells. As well as with enhancing the number of cells the resonance frequencies have increased

b Reflection coefficient (S_{11}) response of the antenna as a function of the slit length. The slit width was kept fixed at 0.3 mm

c Reflection coefficient (S_{11}) response of the antenna as a function of the slit width. The slit length was fixed at 2.3 mm

d Antenna gain versus frequency with variation in number of unit cells ($n = 1$–4 are in simulations and $n = 5$ is in measurements)

e Antenna efficiency versus frequency with variation in number of unit cells ($n = 1$–4 are in simulations and $n = 5$ is in measurements)

f Gain and efficiency response as a function of spiral widths (W_{SP}), distances between spiral rings (S_{SP}) and number of spiral turns (N_{SP}) ($N_{SP} = 1$ and $N_{SP} = 2$ are for simulated and measured cases, respectively)

4 Comparisons

It is well known that the design procedures of both antennas are thoroughly similar, but the antennas layouts, that is, L and F shapes, thickness of their substrates and number of their radiation cells are different from each other, so these differences lead to changing in the antennas performance parameters such as dimensions, bandwidths and radiation specifications (Figs. 7 and 8). The small size, wide bandwidth, desired resonance frequencies and good radiation specifications have been provided by selecting the proper number of structural cells, regulating and optimising the dimensions of radiation cells, that is, sizes of L- and F-shaped slits and spirals along with feed line length, distance between inductive and capacitive elements to the ground plane and distance of the

Table 1 Structural parameters

Parameters	L-shaped antenna	F-shaped antenna
number of cells	4	5
length of slit	2.5	2.3
width of slit	0.3	0.3
width of spiral	0.2	0.2
spacing of spiral	0.2	0.2
number of spiral turns	2	2
length of stub	1.2	1.2
width of stub	0.2	0.2
height of via	0.8	1.6
width of via	0.4	0.3
diameter of via	0.3	0.3
size of unit cells	$2.3 \times 4.9 \times 0.8$ mm^3 $0.0015\lambda_0 \times 0.0032\lambda_0 \times 0.00053\lambda_0$ at 200 MHz	$2.06 \times 4.4 \times 1.6$ mm^3 $0.00075\lambda_0 \times 0.0016\lambda_0 \times 0.00058\lambda_0$ at 110 MHz

Unit in millimetres

Table 2 Design components

Components	L-shaped antenna	F-shaped antenna
C_L, pF	5.8	5.6
L_L, nH	6.2	6
C_R, pF	2.7	2.5
L_R, nH	3.6	3.4
R_L, Ω	2.05	1.85
G_L, υ	2.3	2.15
R_R, Ω	1.25	1.1
G_R, υ	1.5	1.35

Magnitudes of the CRLH-TL unit cell parameters were determined from simulation. Since the implemented spirals in both structures have same layouts with same dimensions (previous table), as a result the differences in L_L are due to variation in height of via holes, which connect the spirals to ground plane (Figs. 3 and 5)

elements to each other, spirals turns, size of the metallic via holes and dimension and characteristics of the substrate. The antennas specifications are listed in Tables 1–3.

According to Table 3, the highest gains and efficiencies of the L- and F-shaped antennas occur at operational resonance frequencies of 1550 and 1900 MHz, which are 3.4 dBi–88% and 4.5 dBi–95%, respectively. Moreover, the minimum amounts of these parameters are 0.5 dBi–21% for L-shaped antenna and 0.3 dBi–18% for F-shaped antenna happened at operating frequencies of 200 and 110 MHz, respectively. Moreover, it can be seen from this table that second design exhibits ~20% bandwidth more than first design. This is mainly due to on enhancing its unit cells from 4 to 5 compared with first version of proposed designs (Figs. 7*a* and 8*a*). Another consequence of this increase is the rise in the number of resonance frequencies of 4 to 5. As well as, increasing the thickness of the same substrate of 0.8–1.6 mm has positive effects on the antenna performance parameters such as dimensions, bandwidth and radiation characteristics. Please note that by increasing the number of unit cells of both antennas we can increase the effective cross-sectional area of them, hence maximum of their gains and efficiencies can enhance to more than 3.4 dBi–88% and 4.5 dBi–95%, respectively for L and F antennas (Figs. 7 and 8), but due to on size limitation a maximum size of 14×5 mm^2 is requested by authors for desired radio applications. Consequently, the optimised number of cells have selected to 4 and 5 cells for the proposed L and F antennas.

It is observed from the antennas specifications that they have benefits of miniaturised dimensions sufficient for fit on the integrated devices and RF embedded systems, wide bandwidth for operating in the VHF and UHF bands, good gains and efficiencies, omnidirectional radiation patterns in the *x*–*z*-plane and monopole such as patterns in the *x*–*y*-plane, low profile, light weight, ease of designing and fabricating and ability for using in wide applications by changing the configurations of the proposed radiation resonating cells based on MTM. Hence, the proposed MTM

Table 3 Performance parameters

Properties	L-shaped antenna	F-shaped antenna
dimension	$13.4 \times 4.9 \times 0.8$ mm^3 $0.0089\lambda_0 \times 0.0032\lambda_0 \times 0.00053\lambda_0$ at 200 MHz	$14.5 \times 4.4 \times 1.6$ mm^3 $0.0053\lambda_0 \times 0.0016\lambda_0 \times 0.00058\lambda_0$ at 110 MHz
bandwidth	200–1800 MHz, 160%	110–2100 MHz, 180.1%
gain, dBi	0.5, 1.2, 1.7, 2.1, 3.4 and 3.0	0.3, 1.0, 1.8, 2.5, 3.8, 4.5 and 4.1
efficiency, %	21, 34, 45, 62, 88 and 80	18, 31, 47, 70, 89, 95 and 90

Gains and efficiencies are at 200, 600, 850, 1200, 1550 and 1800 MHz for L-shaped antenna and at 110, 450, 725, 1150, 1670, 1900 and 2100 MHz for F-shaped antenna

antennas are not limited only to these configurations, so that they can be designed with various layouts for use in the desired applications. Therefore, the fabricated antennas can be good candidates for use in VHF and UHF bands for the wireless communication systems and the radio transceivers.

To validate the design processes of the proposed antennas, their specifications in comparison with other conventional antennas have been summarised in Table 4.

As will be shown in the following, the designs are done using computer simulation. In carrying out the designs in simulations, the antennas are fed directly with a signal source without using a feeding cable. However, when the final designs are completed and prototyped for measurements, a feeding cable is normally used to connect the antennas to the measurement system. Simulations and measurements have been carried out by means of the *HFSS* commercial software and the *Agilent 8722ES* vector network analyser, respectively. The proposed antennas were fabricated by the standards manufacturing techniques based on MTM technology on the engraved circuit boards, and eventually the antennas have been tested in the antenna, microwave and millimetre wave laboratories. After measurement tests, it was found that the simulated results obtained from HFSS full-wave simulator have good agreement with the experimental data.

5 Conclusions

Designing the radiation resonating cells based on MTM-TLs for antenna devices with applications in VHF and UHF bands for wireless communications and radio transceivers has been investigated. With cascading the proper number of the proposed CRLH cells, the desired antenna structures with good properties can be provided. The radiation cells have capability for changing their configurations for use in the wide applications. The designs have been selected as the L- and F-shaped slits, which are engraved on the radiation patches, along with spirals for modelling the desired radiation unit cells, so the slits and spirals play the roles of C_L and L_L, respectively. Moreover, the designs have been shown that by adding a radiation cell can extend the antenna size, consequently the antenna bandwidth and radiation properties have been increased. Moreover, by increasing the thickness of same substrate a good improvement in the performance parameters is observed.

The proposed L- and F-shaped radiation cells were easily designed, tooled and fabricated, so that copper artworks have been engraved directly on the engraved circuit boards using the standard manufacturing techniques, while offer manufacturers faster time to market and reduced bills-of-materials due to the simplified designs. These techniques also offer a greatly reduced need for fabrication and assembly of the antennas components. The resulted antennas from the presented ways can support all cellular frequency bands of 200 MHz–1.8 GHz and 110 MHz–2.1 GHz in VHF and UHF bands for radio transceivers, using single or multiple feed designs, which eliminate the need for antenna switches. Moreover, the proposed antennas with low profiles and miniaturised dimensions can be flush-mounted on various structures including vehicles, cellular base stations, mobile

Table 4 Comparison of the antenna characteristics

Papers	Dimensions	Bandwidth	Gain (max), dBi	Efficiency (max), %
[11] b-shaped antenna with 4UC	*ES*:$0.047\lambda_0 \times 0.021\lambda_0 \times 0.002\lambda_0$ at 1 GHz *PHS*:$14.2 \times 6.32 \times 0.8$ mm^3	1–3.2 GHz (104.76%)	2.3	62
[11] b-shaped antenna with 6UC	*ES*:$0.051\lambda_0 \times 0.016\lambda_0 \times 0.002\lambda_0$ at 800 MHz *PHS*:$19.2 \times 6.32 \times 0.8$ mm^3	0.8–3.4 GHz (123.8%)	2.8	70
[12] J-shaped antenna with 8UC	*ES*:$0.564\lambda_0 \times 0.175\lambda_0 \times 0.02\lambda_0$ at 7.5 GHz *PHS:* $22.6 \times 7 \times 0.8$ mm^3	7.25–17.8 GHz (84.23%)	2.3	48.2
[12] l-shaped antenna with 7UC	*ES*:$0.556\lambda_0 \times 0.179\lambda_0 \times 0.041\lambda_0$ at 7.7 GHz *PHS:* $21.7 \times 7 \times 1.6$ mm^3	7.8–19.85 GHz (87.16%)	3.4	68.1
[12] J-shaped antenna with 6UC	*ES:* $0.45\lambda_0 \times 0.175\lambda_0 \times 0.02\lambda_0$ at 7.5 GHz *PHS:* $18 \times 7 \times 0.8$ mm^3	7.5–16.8 GHz (74.4%)	2.1	44.3
[12] l-shaped antenna with 5UC	*ES:* $0.428\lambda_0 \times 0.179\lambda_0 \times 0.041\lambda_0$ at 7.7 GHz *PHS:* $16.7 \times 7 \times 1.6$ mm^3	7.7–18.6 GHz (82.88%)	3.1	58.6
[14]	*ES:* $0.134\lambda_0 \times 0.035\lambda_0 \times 0.002\lambda_0$ at 670 MHz *PHS:* $60 \times 16 \times 1$ mm^3	0.67–2.55 GHz (116.7%)	4.74	62.88
[15]	*ES:* $0.108\lambda_0 \times 0.108\lambda_0 \times 0.009\lambda_0$ at 1.8 GHz *PHS:* $18 \times 18 \times 1.6$ mm^3	1.8–2.35 GHz (26.5%)	3.69	20
[16]	*ES:* $0.164\lambda_0 \times 0.013\lambda_0 \times 0.013\lambda_0$ at 800 MHz *PHS:* $60 \times 5 \times 5$ mm^3	0.8–2.5 GHz (103.03%)	0.45	53.6
[17]	*ES:* $0.06\lambda_0 \times 0.06\lambda_0 \times 0.021\lambda_0$ at 1 GHz *PHS:* $18.2 \times 18.2 \times 6.5$ mm^3	1–2 GHz (66.66%)	0.6	26
proposed L-shaped antenna with 4UC	*ES*:$0.0089\lambda_0 \times 0.0032\lambda_0 \times 0.00053\lambda_0$ at 200 MHz *PHS:* $13.4 \times 4.9 \times 0.8$ mm^3	0.2–1.8 GHz (160%)	3.4	88
proposed F-shaped antenna with 5UC	*ES*:$0.0053\lambda_0 \times 0.0016\lambda_0 \times 0.00058\lambda_0$ at 110 MHz *PHS*:$14.5 \times 4.4 \times 1.6$ mm^3	0.11–2.1 GHz (180.1%)	4.5	95

UC: unit cells, ES: electrically size and PHS: physically size

handsets, RF embedded circuits and integrated devices for use in the wireless communication systems.

The proposed designs are not just limited to the offered shapes of slits, that is, L and F configurations. So that by modelling these slits with other layouts can be realised the various structures for use in the wide applications. This point is main feature of the proposed designs.

6 References

1 Anguera, J., Andújar, A., Huynh, M.C., *et al.*: 'Advances in antenna technology for wireless handheld devices', *Int. J. Antennas Propag.*, 2013, **2013**, Article ID 838364
2 Caloz, C., Itoh, T.: 'Electromagnetic metamaterials: transmission line theory and microwave applications' (Wiley, New York, 2006)
3 Engheta, N., Ziolkowski, R.W.: 'Metamaterials: physics and engineering explorations' (Wiley, New York, 2006)
4 Caloz, C., Itoh, T.: 'Electromagnetic metamaterials: transmission line theory and microwave applications, the engineering approach' (John Wiley & Sons, New York, 2005)
5 Shelby, R.A., Smith, D.R., Schultz, S.: 'Experimental verification of a negative index of refraction', *Science*, 2001, **292**, (5514), pp. 77–79
6 Lee, C.J., Achour, M., Gummalla, A.: 'Compact metamaterial high isolation MIMO antenna subsystem'. Proc. Asia Pacific Microwave Conf., 2008, pp. 1–4
7 Lee, C.J., Leong, K.M.H., Itoh, T.: 'Broadband small antenna for portable wireless application'. Int. Workshop on Antenna Technology: Small Antennas and Novel Metamaterials, iWAT 2008, 4–6 March 2008, pp. 10–13
8 Alibakhshi-Kenari, M., Movahhedi, M., Naderian, H.: 'A new miniature ultra wide band planar microstrip antenna based on the metamaterial transmission line'. IEEE Asia-Pacific Conf. on Applied Electromagnetics, Melaka, Malaysia, 11–13 December 2012
9 Alibakhshi-Kenari, M.: 'A new compact UWB traveling-wave antenna based on CRLH-TLs for embedded electronic systems', *Int. J. Microw. Wirel. Technol.*, 2014, pp. 1–4, doi: http://www.dx.doi.org/10.1017/S1759078714001020
10 Jackson, J.D.: 'Classical electromagnetics' (John Wiley & Sons, New York, 1999, 3rd edn.)
11 Alibakhshi-Kenari, M.: 'Printed planar patch antennas based on metamaterial', *Int. J. Electron. Lett.*, 2014, pp. 37–42, doi: http://www.dx.doi.org/10.1080/21681724.2013.874042
12 Alibakhshi-Kenari, M.: 'Introducing the new wide band small plate antennas with engraved voids to form new geometries based on CRLH MTM-TLs for wireless applications', *Int. J. Microw. Wirel. Technol.*, 2014, **6**, (06), pp. 629–637
13 Ansoft HFSS. Available at http://www.ansoft.com/products/hf/hfss
14 Luo, J., Gong, S., Duan, P., *et al.*: 'Small-size wideband monopole antenna with CRLH-TL for LTE mobile phone', *Prog. Electromagn. Res. C*, 2014, **50**, pp. 171–179
15 Abdalla, M.A., Awad, A.A., Hassan, K.M.: 'Wide band high selective compact metamaterial antenna for 2 GHz wireless applications'. Antennas and Propagation Conf. (LAPC), Loughborough, 10–11 November 2014, pp. 350–354
16 Li, Y., Zhang, Z., Zheng, J., *et al.*: 'Compact heptaband reconfigurable loop antenna for mobile handset', *IEEE Antennas Wirel. Propag. Lett.*, 2011, **10**, pp. 1162–1165
17 Lee, C.J., Leong, K.M.K.H., Itoh, T.: 'Composite right/left-handed transmission line based compact resonant antennas for RF module integration', *IEEE Trans. Antennas Propag.*, 2006, **54**, (8), pp. 2283–2291